Amino acid substitutions in norovirus VP1 dictate cell tropism via an attachment process dependent on membrane mobility.

Jake T. Mills[1], Susanna C. Minogue[1], Joseph S. Snowden[1], Wynter K.C. Arden[2], David J. Rowlands[1], Nicola J. Stonehouse[1], Christiane E. Wobus[2], and Morgan R. Herod[1]*

* corresponding author m.r.herod@leeds.ac.uk

[1] Astbury Centre for Structural Molecular Biology, School of Molecular & Cellular Biology, Faculty of Biological Sciences, University of Leeds, Leeds, UK.

[2] Department of Microbiology and Immunology, University of Michigan Medical School, Ann Arbor, MI 48130, USA.

Running title: Cellular tropism of norovirus

Keywords: MNV, murine norovirus, CD300lf, receptor, membrane fluidity, virus evolution

Word/Figure count: 4953 words, 5 figures, 239 words abstract, 150 importance

Abstract

Viruses interact with receptors on the cell surface to initiate and co-ordinate infection. The distribution of receptors on host cells can be a key determinant of viral tropism and host infection. Unravelling the complex nature of virus-receptor interactions is, therefore, of fundamental importance to understanding viral pathogenesis. Noroviruses are non-enveloped, icosahedral, positive-sense RNA viruses of global importance to human health, with no approved vaccine or antiviral agent available. Here we use murine norovirus as a model for the study of molecular mechanisms of virus-receptor interactions. We show that variation at a single amino acid residue in the major viral capsid protein had a key impact on the interaction between virus and receptor. This variation did not affect virion production or virus growth kinetics, but a

specific amino acid was rapidly selected through evolution experiments, and significantly improved cellular attachment when infecting immune cells in suspension. However, reducing plasma membrane mobility counteracted this phenotype, providing insight into for the role of membrane fluidity and receptor recruitment in norovirus cellular attachment. When the infectivity of a panel of recombinant viruses with single amino acid variations was compared *in vivo*, there were significant differences in the distribution of viruses in a murine model, demonstrating a role in cellular tropism *in vivo*. Overall, these results highlight the importance of lipid rafts and virus-induced receptor recruitment in viral infection, as well as how capsid evolution can greatly influence cellular tropism, within-host spread and pathogenicity.

Importance

All viruses initiate infection by utilising receptors to attach to target host cells. These virus-receptor interactions can therefore dictate viral replication and pathogenesis. Understanding the nature of virus-receptor interactions could also be important to developing novel therapies. Noroviruses are non-enveloped icosahedral viruses of medical importance. They are a common cause of acute gastroenteritis with no approved vaccine or therapy and are a tractable model for studying fundamental virus biology. In this study, we utilise the murine norovirus model system to show that variation in a single amino acid of the major capsid protein can alone can affect viral infectivity through improved attachment to suspension cells. Reducing plasma membrane mobility reduced infectivity, providing an insight into the importance of membrane mobility for receptor recruitment. Furthermore, variation at this site was able to change viral distribution in a murine model, illustrating how in-host capsid evolution can influence viral infectivity and immune evasion.

Introduction

Cellular tropism is a key determinant for viral infection of a host and is dictated by several factors, including viral attachment to cellular receptors. Unravelling the complex nature of virus-receptor interactions is therefore of fundamental importance to understanding viral pathogenesis. Human noroviruses (HNV) cause gastroenteritis and are responsible for >200,000 deaths and a cost of ~£40 billion worldwide each year (1). With no efficacious vaccine or approved therapy to treat HNV infections, a greater understanding of the virus life cycle and capsid structure is likely to be important for developing new approaches to disease control.

Noroviruses are members of the *Caliciviridae* family of positive-sense single-stranded RNA viruses (1), that have three or four open reading frames (ORF) 1-4 (2). ORF1 is translated to produce the viral polyprotein that is cleaved to generate the non-structural (NS) proteins required for genome replication (2). ORF2 and 3 encode the two viral structural proteins, VP1 and VP2, respectively (2). ORF4 is only expressed in murine norovirus (MNV) and encodes virulence factor 1 (VF1) (3). The two viral structural proteins assemble to enclose the genome in a *T = 3* capsid. This protein shell is ~40 nm in diameter and is composed of 180 copies (90 dimers) of the major structural protein VP1, and a low copy number of the minor structural protein VP2 (4). In feline calicivirus, 12 copies of VP2 forms a portal-like assembly likely involved in genome release, but this is yet to be demonstrated for other caliciviruses (4). VP1 monomers comprise an N-terminal region, a shell (S) domain, and a protruding (P) domain. The P domain is additionally split into the proximal and distal sub-domains, P1 and P2, respectively (5, 6). *In vitro* replication of HNV has been demonstrated in human intestinal enteroids (7), human B cells (8) and salivary gland cells (9), but these models are technically challenging, highly variable (10), and

suffer from the lack of an effective reverse genetics system. Consequently, MNV is frequently used as a model system for the study of norovirus structure and pathology.

MNV is widely prevalent in laboratory mice (11). MNV-1 was the first strain of MNV to be identified (12), and it establishes acute, self-resolving infections in wild-type mice, but can be fatal in immune compromised ($STAT1^{-/-}$) mice (13). Different strains of MNV have different cellular tropisms, which in turn determine the site(s) of infection in the host. Strains such as MNV-3 are located primarily in the colon and caecum (14), while MNV-1 is detected across the gastrointestinal tract and in immune cells (15), including macrophages and dendritic cells, thought to aid virus distribution to extra-intestinal sites (16–18). Furthermore, MNV-3 can still be detected in the faeces 56 days post-infection and can establish lifelong persistent infections (14). This draws parallels with HNV infection, whereby virus shedding can be detected up to 28 days post-infection (19), and persistent infection in immunocompromised individuals can last years (20). Cellular tropism is also important in determining MNV persistence, with serotypes such as MNV-CR6 able to infect rare tuft cells located in the intestinal epithelium and evade the immune system (21, 22).

The cellular tropism of MNV is thought to be determined by expression of CD300lf, the primary proteinaceous receptor (with the virus also able to utilise CD300ld to enter the cell) (24, 25). Both CD300lf and CD300ld are members of the CD300 receptor family of type I transmembrane proteins with a 2 disulphide bond extracellular domain (26). They are present on numerous immune cell types such as dendritic cells, where they are thought to play opposing roles to maintain homeostasis (24, 27). Since the identification of CD300lf as the physiological

receptor for MNV (28), studies have begun to dissect the nature of this interaction. The P2 sub-domain of the VP1 capsid directly interacts with the receptor, with two CD300lf ectodomains binding one P2 sub-domain (25). The interaction mimics the way phospholipids bind to the receptor, is conserved across multiple MNV serotypes, and is enhanced by divalent cations (Ca^{2+} and Mg^{2+}) and bile acid (25, 29, 30). Structural studies have suggested that up to 21 amino acids of VP1 form a network of interactions with 19 residues of CD300lf (5, 24, 25). Despite this extensive network of interactions, the binding affinity is reported to be low (KD:~219 μM), therefore, receptor avidity may be important for endocytosis (25). Studies have attempted to elucidate how genetic variation in VP1 can influence cellular tropism and pathogenesis (23, 31–33), however more research is needed.

Using the MNV model system, we demonstrate that variation in a single amino acid in the major capsid protein can alter virus-receptor interactions in cell culture, as well as within-host spread in the mouse model. Specifically, our experiments suggest that a single substitution at this site can enhance cell specific growth in culture by allowing more robust recruitment of multiple receptors under conditions of high membrane fluidity. Consistent with this idea, reducing membrane mobility significantly reduced viral infection. Finally, this amino acid variation affects tissue tropism in mice, which has implications for within-host spread and organ-specific infection. Together, these results reveal information on how viruses utilise membrane fluidity to overcome low-affinity receptor interactions, and how the plasticity of the viral capsid can affect cellular and organ tropism.

Results

Identification of key residues in VP1 for MNV infectivity

Previous studies identified 21 amino acids of MNV VP1 that form a network of interactions with the receptor CD300lf (24, 25, 34). Through alignment of all available MNV sequences, most of these residues are highly or completely conserved across MNV isolates, however, one residue, VP1 301, showed considerable variability (Figure 1A). Furthermore, we noted that there was an association between the residue encoded in this position and viral strains, i.e. MNV-1 and MNV-4 predominantly encode threonine (T) whilst all other strains predominantly encode isoleucine (I). We therefore set out to investigate how variations in the identity of this VP1 residue could influence viral replication and pathogenesis.

We began by investigating whether variants at this amino acid position were genetically stable through cell culture evolution experiments. To ensure a homogenous genetic background, we modified an infectious clone of MNV-1.CW1 (that encodes T at amino acid 301 of VP1), to encode either, I, valine (V), or proline (P). All of these amino acids have been documented at this position in MNV sequences deposited to GenBank. In order to ascertain the importance of the amino acid at this position, we also generated infectious clones with serine (S), leucine (L), aspartic acid (D) or lysine (K). These infectious clones were used to produce *in vitro* transcribed RNA and virus was recovered by transfection of BHK-21 cells (termed passage 0). The recovered viruses were serially passaged 10 times in BV-2 cells grown adherently or in suspension (for brevity termed BV-2S). RNA was extracted from virus samples taken at indicated passages, reverse transcribed, and the consensus ORF2 sequence determined (Figure 1B and C).

When passaged in adherent BV-2 cells (Figure 1B), the VP1 sequence for the MNV-1.CW1 infectious clones carrying T301, V301, S301 and L301 did not change throughout the experiment. With the I301 infectious clone, two out of the three replicates maintained I301 at passage 10, whilst an I301L substitution occurred in the third replicate by passage 10. MNV-1.CW1 infectious clones carrying P301, D301 and K301 all underwent substitution at this position by passage 6 to encode a range of amino acids, which narrowed by passage 10 to P301T, D301V/S and K301T/V. For all of the sequences there were no other amino acid changes throughout ORF2.

In BV-2S cells, only the MNV-1.CW1 I301 infectious clone was stable and did not acquire any VP1 amino acid substitutions throughout the experiment (Figure 1C). In contrast, substitutions were found in MNV-1.CW1 T301, S301 and L301 infectious clones to encode isoleucine at the consensus level (T301I, S301I and L301I) between passage 5 and 7 (Figure 1C). Again, in infectious clones of MNV-1.CW1 encoding D301 or K301, substitution of D301V/I and K301L/T in the consensus sequence was detected by passage 5 (Figure 1C). Importantly, there were no other changes to the wild-type sequence of MNV-1.CW1 VP1 in any of the infectious clones. To determine the effects of these substitutions on viral yield, supernatants from the BV-2S passage experiment were titrated by $TCID_{50}$ assay on BV-2 cells (Figure 1D).

The titre of the MNV-1.CW1 I301 clone increased over the duration of the experiment from ~$1x10^4$ $TCID_{50}$/mL at passage 1 to ~$1x10^8$ $TCID_{50}$/mL by passage 10, which was the peak titre for any virus. Infectious clones carrying MNV-1.CW1 T301, S301, and L301 (that all changed to 301I) followed a similar pattern, having initial titres between $1x10^3$ - $1x10^4$ $TCID_{50}$/mL, before increasing to ~$1x10^7$ $TCID_{50}$/mL

by passage 10. The infectivity of MNV-1.CW1 D301 and K301 were below the limit of detection (LOD) until passage 5, when the titre increased to ~$1x10^4$ and ~$1x10^5$ $TCID_{50}$/mL, respectively, before the titre reached a peak of ~$1x10^7$ $TCID_{50}$/mL at passage 10. This increase in titre coincided with the change to hydrophobic residues, with a preference for 301I. Together, these data suggest that viruses with isoleucine at VP1 position 301 have a particular advantage when grown in suspension cell culture.

A)

Amino Acid at VP1 301	Frequency (%)
Threonine	79
Isoleucine	13
Valine	5
Proline	2
Methionine	1

B)

BV-2 Cells

Passage 0	Passage 6	Passage 10
I	I	I / L
T	T	T
V	V	V
P	T	T
S	S	S
L	L	L
D	V / S	V / S
K	I / T / L	T / V

C)

BV-2S Cells

Passage 0	Passage 5	Passage 7	Passage 10
I	I	I	I
T	T	T / I	I
S	S	I	I
L	L	I	I
D	V / _	V / I	V / I
K	L / I	L / I	L / I

D)

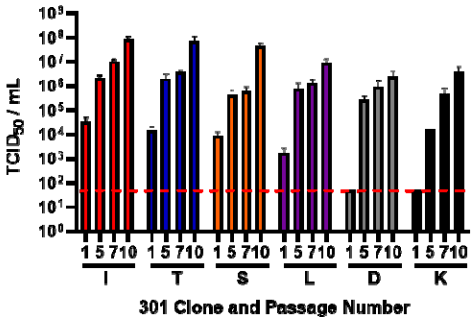

Figure 1: Repeat passaging of MNV-1 in suspension leads to selection of hydrophobic residues at VP1 301. (A) Overall amino acid variation at MNV VP1 301 was plotted from deposited sequences on GenBank. Recombinant MNV-1.CW1 with single amino acid substitutions in the infectious clones were passaged 10 times in **(B)** adherent BV-2 cells or **(C)** BV2 cells in suspension (BV-2S), before the ORF2 was sequenced at indicated passages. Data shows amino acid residues encoded at the position 301 of VP1 (n = 3). **(D)** Viruses passaged through BV-2S cells were titrated at selected passages as indicated. Red dotted line demonstrates limit of detection for $TCID_{50}$ assay. Data shows mean $TCID_{50}$/mL (n = 3 ± SEM).

The VP1 301 amino acid is a major determinant for infectious virus production in suspension cultures

To confirm that VP1 I301 conferred increased viral infectivity in suspension cell culture, the virus yield following transfection of BHK-21 cells with RNA was determined in BV-2 cells. RNA transcribed *in vitro* from the infectious clones was transfected into BHK-21 cells which are permissive for viral replication but do not express the viral receptor, therefore the amount of infectious virus detected is directly proportional to the replication of the transfected RNA alone. Virus was collected and titrated by $TCID_{50}$ assays on suspension grown BV-2S cells (Figure 2A), adherently grown BV-2 cells (Figure 2B) or BV-2 cells grown adherently but infected in suspension (Figure 2C). For suspension $TCID_{50}$ assays, viral dilutions were prepared and added to the plates first, before cells were seeded.

On BV-2S cells (Figure 2A), the titre of the MNV-1.CW1 I301 variant was significantly higher than all other infectious clones. This was ~5-fold higher than MNV-1.CW1 V301 and S301 and ~10-fold greater than MNV-1.CW1 T301, L301 and D301. Both MNV-1.CW1 P301 and K301 variants had titres below the LOD, suggesting these substitutions are detrimental to MNV infectivity.

In contrast, when the infectious clones were titrated on adherently grown BV2 cells (Figure 2B), there were no significant differences in the titre of MNV-1.CW1 S301, I301, T301, V301, L301 and D301 viruses, with titres all between $1x10^5$ $TCID_{50}$/mL and $1x10^6$ $TCID_{50}$/mL. Again, MNV-1.CW1 P301 and K301 were highly detrimental for infectivity.

To understand whether this observation was specific for cells grown or infected in suspension, the $TCID_{50}$ assays were repeated with adherently grown BV-2 cells, however, the infection was performed while the cells were in suspension before

being allowed to adhere to the culture vessels (Figure 2C). In this setup, the titre of the MNV-1.CW1 I301 variant was again significantly higher than all other infectious clones, except MNV-1.CW1 S301, with both titres ~10-fold greater than for MNV-1.CW1 T301, V301, L301 and D301 variants. Once again, MNV-1.CW1 P301 and K301 viral recovery was at or below the LOD.

To rule out differences in transfection efficiency, we conducted similar experiments whereby select infectious clone RNA was co-transfected into BHK-21 cells alongside an IRES-GFP DNA plasmid. The measurement of GFP fluorescence alongside titration of the recovered virus allowed us to correct the viral titre for variation in transfection efficiency. Following collection, the virus was titred by $TCID_{50}$ assay in the same three cell infection conditions and normalised to GFP fluorescence at 24 hours post-transfection.

Once again, MNV-1.CW1 I301 had a significantly greater viral titre compared to all other infectious clones when the $TCID_{50}$ assay was conducted in BV-2S cells (Supplemental Figure 1A). There was no significant difference in viral titres between infectious clones in adherent BV-2 cells (Supplemental Figure 1B). Although there was no significant difference in adherent BV-2 cells infected in suspension (Supplemental Figure 1C), there was a similar pattern to BV-2S cells across the infectious clones.

Taken together, our data suggest that the MNV-1.CW1 I301 variant has a selective advantage at infecting cells when in suspension, but no selective advantage is observed in adherent cells. To determine whether the differences between MNV-1.CW1 I301 and MNV-1.CW1 T301 viruses applied to another cell type, cell culture infectivity assays were performed in the suspension-grown mouse B lymphocyte cell line WEHI-231. Cells were infected as before and an MTS assay was used to

239 determine cell viability and thus calculate virus infectivity ($TCID_{50}$ assays could not
240 be performed as WEHI-231 cells do not adhere to tissue culture plates; Figure 2D).
241 The viral titre of MNV-1.CW1 I301 was ~5-fold greater compared to MNV-1.CW1
242 T301. In comparison, an infectious clone carrying a replication-defective mutation in
243 the viral polymerase (GNN) (35) had viral recovery below the LOD.
244 One possible explanation for our observations is that some of the VP1 301 variations
245 affect virion assembly, not receptor engagement. To investigate this, the total
246 production of viral particles was measured by one step RT-qPCR. Virus was
247 produced from infectious clone RNA by transfection into BHK-21 cells as before, and
248 non-encapsidated RNA was degraded by nuclease treatment before RNA was
249 extracted and the protected RNA concentration measured by one-step RT-qPCR
250 (Figure 2E). There were no statistically significant differences in the number of virus
251 particles produced by any of the clones.
252 Taken together, these data indicate that the VP1 301 residue plays an important role
253 in MNV infection, but that this is unrelated to viral replication.

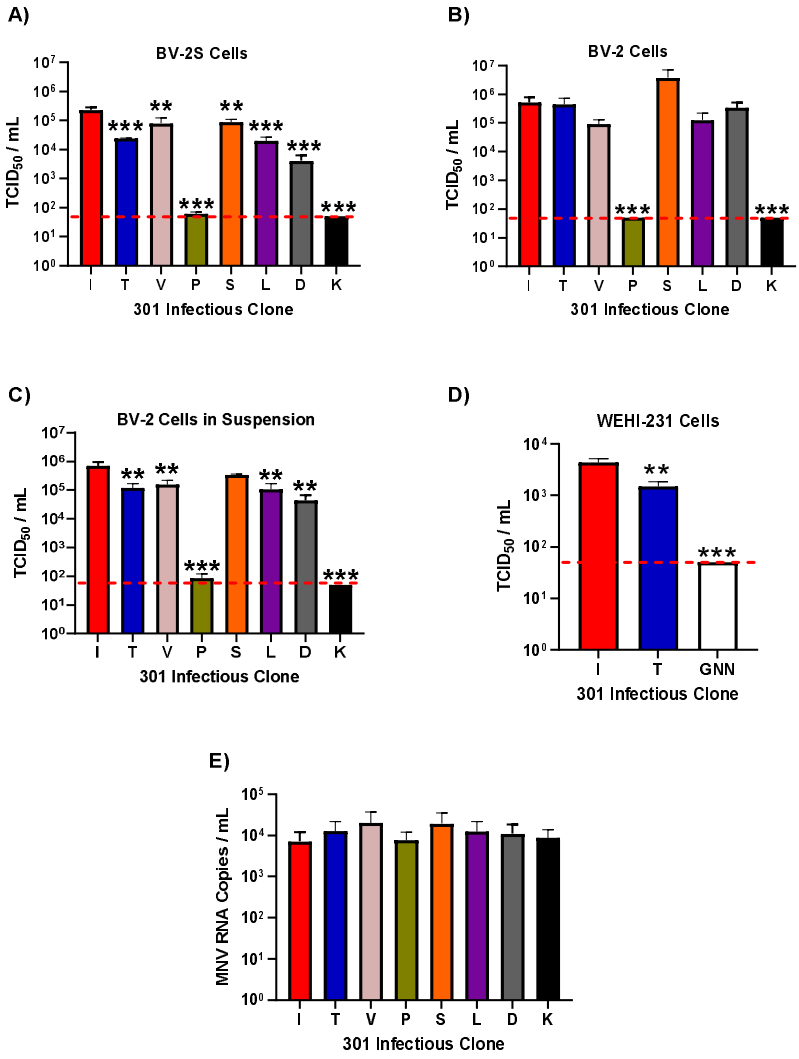

Figure 2: The VP1 301 residue is a major determinant of virus particle infectivity *in vitro*. MNV-1.CW1 infectious clone RNAs with the indicated amino acids at VP1 301 were transfected into BHK-21 cells and virus-containing supernatants collected after 48 hours. Virus titre was determined by $TCID_{50}$ assays on **(A)** suspension BV-2S cells, **(B)** adherent BV-2 cells, **(C)** adherent BV-2 cells infected in suspension or **(D)** WEHI-231 B lymphocyte suspension cells. The WEHI-231 experiment also contained an RdRp replication-defective MNV GNN negative control. Data shows mean $TCID_{50}$/mL, with significance compared to I301 using one-way ANOVA with corrections for multiple comparisons (n = 3 ± SEM, *p<0.05;

264 **p<0.01; ***p<0.001). The red dotted line demonstrates limit of detection for $TCID_{50}$
265 assays. **(E)** In separate transfections, the recovered supernatant was treated with 25
266 U/mL benzonase for 30 minutes at 37□C, before RNA was extracted. RNA
267 concentration was then measured by one-step RT-qPCR. Data show mean RNA
268 genome copies/mL (n = 3 ± SEM).

The amino acid at VP1 301 affects cell attachment

VP1 residue 301 contributes to the virus-CD300lf receptor interface (25) and our data suggested that variation in this amino acid alone is sufficient to confer a replicative advantage to the virus. We hypothesised that the VP1 I301 variant has greater affinity for the receptor, thus increasing cell attachment. To investigate this hypothesis, we conducted virus binding assays with the MNV-1.CW1 I301 or T301 variants on BV-2S cells. We expected that the MNV-1.CW1 I301 variant would bind more effectively to cells in suspension compared to viruses encoding hydrophilic residues.

To prevent endocytosis, binding assays were conducted on BV-2S cells treated with dynasore (Ds), an inhibitor of dynamin that is required for MNV internalisation (36). BV-2S cells were pre-treated with Ds at 37□C, or left untreated as a control, prior to incubation with MNV-1.CW1 I301 or T301 viruses. The amount of virus attached to the cells was measured by western blot for the major viral structural protein, VP1. When analysed by western blot (Figure 3A) and normalised to GAPDH expression, significantly more MNV-1.CW1 I301 binding was detected compared to MNV-1.CW1 T301 in the Ds pre-treated cells (Figure 3B). There was also a trend of increased binding of MNV-1.CW1 I301 compared to MNV-1.CW1 T301 in untreated cells, but this was not statistically significant. BSA was used as a loading control for supernatant, due to the presence of FCS (which contains BSA) in the cell media.

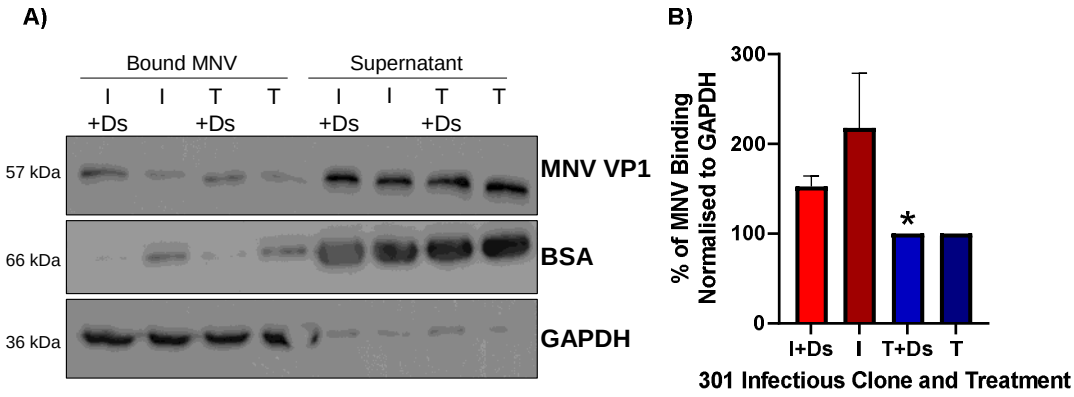

289 **Figure 3: MNV I301 has greater binding capacity than MNV T301 to BV-2S cells.**
290 **(A)** BV-2S cells were untreated or pre-incubated with 50 µM dynasore (Ds) for 30
291 minutes at 37□C, before MNV-1.CW1 I301 or MNV-1.CW1 T301 (MOI 1) was added
292 and incubated for 2 hours at 37□C. Supernatant was removed, cell pellet washed in
293 ice cold PBS before lysis in RIPA buffer. The amount of MNV present in each
294 fraction was quantified by western blot with GAPDH and BSA used as cell-
295 associated and supernatant loading controls, respectively (one representative blot
296 shown). **(B)** The amount of VP1 was quantified by densitometry and normalised to
297 GAPDH. Data shows mean percentage increase/decrease for bound MNV-1.CW1
298 I301 compared to MNV-1.CW1 T301, with significant differences in virus-cell
299 interaction between MNV-1.CW1 I301 and MNV-1.CW1 T301 infectious clones
300 determined using unpaired T-test (n = 3 ± SEM, *p<0.05).

MNV binding is dependent on membrane fluidity

Taken together, our observations suggest that viruses encoding I301 have a selective growth advantage and increased cell attachment when in suspension. To confirm that differences between cell types were not due to differences in replication rates, a one-step growth curve with MNV-1.CW1 T301 (10 PFU/cell) was carried out on BV-2 and BV-2S cells. At 12 hours post-infection, there appeared to be an increase in MNV titre in BV-2S cells (albeit not statistically significant), but at the 24 and 48 hour time-points, there was no difference in viral titre (Supplemental Figure 2A). To address potential differences in CD300lf expression between the cell types, we compared the expression levels of CD300lf receptor in BV-2 and BV-2S cells by western blot (Supplemental Figure 2B). The western blot indicated the presence of multiple CD300lf glycosylation states (75 kDa main isoform), as has been previously described (37, 38), however there was no clear difference in relative expression of these different forms between BV-2 and BV-2S cells. BHK-21 cells were used as a negative control, and L-cells and RAW 264.7 cells were used as positive controls for CD300lf expression. Flow cytometry was also used to calculate CD300lf expression in BV-2 and BV-2S cells (Supplemental Figure 2C). There was no difference in CD300lf receptor expression between adherent or suspension cells, with a clear decrease in fluorescence in the controls with no secondary antibody.

Finally, as suspension cells have a greater plasma membrane fluidity compared to adherent cells (39, 40), we hypothesised that fluidity of the cell membrane may affect MNV binding to the cell. We therefore first reduced membrane mobility by performing the binding assay at a reduced temperature. BV-2S cells were pre-treated with Ds at 37□C (to inhibit internalisation), prior to incubation with MNV-1.CW1 I301 or T301 viruses at either 0□C or 37□C. At reduced temperature there was significantly less

binding of MNV-1.CW1 to cells, such that little or no VP1 could be detected (Figure 4A & 4B). Next, we treated cells with methyl-β-cyclodextrin (MβCD) and losartan (Los), two compounds reported to chemically restrict membrane mobility (41, 42). To conduct this experiment, BV-2S cells were pre-treated with either Ds, MβCD, Ds & MβCD, or left untreated as a control (Figure 4C & 4D) at 37□C, and either Ds, Los, Ds & Los, or left untreated as a control (Figure 4E & 4F), prior to incubation with MNV-1.CW1 I301 or T301 viruses. MβCD (Figure 4C & 4D) and Los (Figure 4E & 4F) both significantly reduced MNV binding in BV-2S cells by approximately 50% and 30%, respectively. Together, the data indicate the importance of plasma membrane fluidity in MNV cell binding.

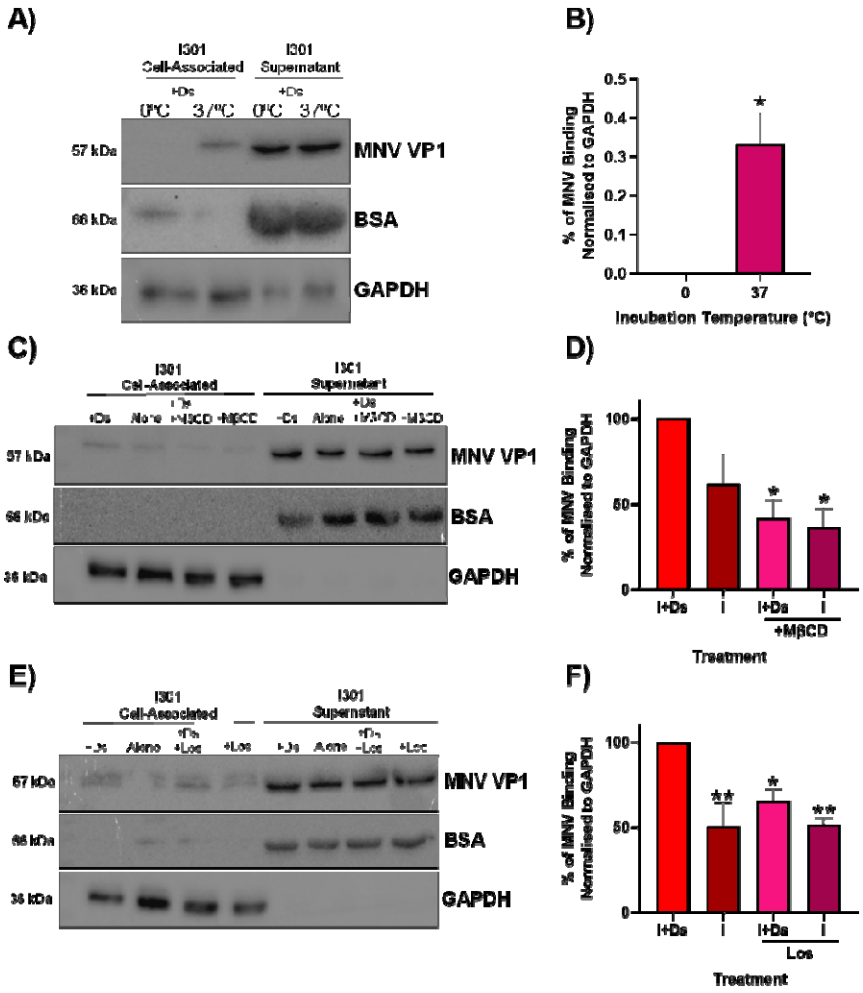

Figure 4: MNV cell binding is temperature dependent and requires membrane fluidity. (A) BV-2S cells were pre-incubated with 50 µM dynasore (Ds) for 30 minutes at 37□C, before MNV-1.CW1 I301 (MOI 1) was added and incubated for 2 hours at 0□C or 37□C. Supernatant was removed, cell pellet washed in ice-cold PBS before lysis in RIPA buffer. The amount of MNV present in each fraction was quantified by western blot with GAPDH and BSA used as cell-associated and supernatant loading controls, respectively (one representative blot shown; n = 3). **(B)** VP1 was quantified by densitometry and normalised to GAPDH. Data shows mean densitometry for bound MNV at 0□C and 37□C, with significant differences in virus-cell interaction between temperatures determined using paired T-test (n = 3 ± SEM,

346 *p<0.05). BV-2S cells were untreated or pre-incubated with **(C)** 50 µM Ds, 2 mM
347 methyl-β-cyclodextrin (MβCD) or both Ds and MβCD for up to 60 minutes at 37□C;
348 or **(E)** 50 µM Ds, 40 mM losartan (Los) or both Ds and Los for 30 minutes at 37□C,
349 before MNV-1.CW1 I301 (MOI 1) was added and incubated for 2 hours at 37□C. The
350 binding assay was then performed as in panel A (one representative blot shown; n =
351 3). The amount of VP1 found was quantified by densitometry and normalised to
352 GAPDH. Data shows mean densitometry for bound MNV, with significant differences
353 in virus-cell interaction between cells **(D)** with or without MβCD pre-treatment; or **(F)**
354 with or without Los pre-treatment determined using one way ANOVA with corrections
355 for multiple comparisons (n = 3 ± SEM, *p<0.05; **p<0.01.)

356 **The amino acid at VP1 301 influences MNV infectivity and tropism *in vivo***

357 Our data suggested that MNV-1.CW1 I301 infected suspension cells more effectively
358 than viruses with other amino acids at this position. We therefore hypothesised that
359 this variation at VP1 301 may affect the cellular tropism in a murine model, due to
360 improved infection of non-adherent immune cells at the early stages of infection. To
361 investigate this, seven-week-old C57BL/6 mice were infected by oral gavage with
362 $3x10^5$ PFU/mouse of MNV-1.CW1 I301 or T301. Tissues were harvested from the
363 jejunum (JE), duodenum (DU), ileum (IL), caecum (CE), spleen (SP) and mesentery
364 lymph nodes (ML) at 12 hours post-infection and MNV titre measured by plaque
365 assay (Figure 5).
366 Both MNV-1.CW1 I301 and T301 were detected in all organs after 12 hours of
367 infection. The MNV-1.CW1 I301 viral titre in the SP was significantly higher
368 compared to MNV-1.CW1 T301. There was also a trend of increased MNV-1.CW1
369 I301 in the ML compared to MNV-1.CW1 T301, and increased MNV-1.CW1 T301 in
370 the IL in comparison to MNV-1.CW1 I301, but these were not statistically significant.
371 To confirm the virus capsid had not undergone mutations during the mouse infection
372 experiments, RNA was extracted from the SP and the sequence of ORF2
373 determined from the recovered virus. There were no changes identified to the ORF2
374 consensus sequence extracted from any of the recovered virus compared to the
375 input viruses used for infection. The mouse data agree with our cell culture
376 experiments and suggest that the single amino acid substitution from T to I at
377 position 301 in VP1 can lead to changes in tissue tropism and viral dissemination in
378 the native host.

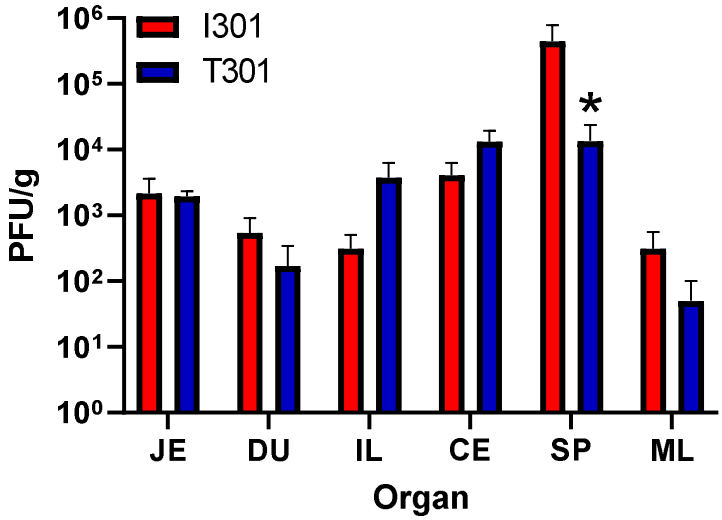

Figure 5: The VP1 301 residue is a determinant of tissue tropism in mice. Seven-week-old C57BL/6 mice were infected by oral gavage with $3x10^5$ PFU/mouse of MNV-1.CW1 I301 or MNV-1.CW1 T301. Mice were sacrificed at 12 hours post-infection, tissues were harvested, and viral titres were determined by plaque assay from the jejunum (JE), duodenum (DU), ileum (IL), caecum (CE), spleen (SP) and mesentery lymph nodes (ML). Plaque numbers (PFU) were normalized to tissue weight (in g). Data show mean PFU/g with significance compared to I301 using two-way ANOVA with corrections for multiple comparisons (n = 5 ± SEM, *p<0.05).

Discussion

MNV has a tropism *in vivo* for adherent intestinal epithelial cells, as well as immune cells (13), which are largely non-adherent. Despite this, MNV infection assays in cell culture are usually conducted on adherent macrophage-like cells, ignoring any consequences of infection of cells in suspension. Our work demonstrates that culture and passage of MNV-1 in suspension selects for a single amino acid substitution at VP1 301 that significantly increases infectivity, due to enhanced binding to BV-2S cells. Furthermore, VP1 301 variations are important for the production of infectious virions. The experiments in mice reported here complement the cell culture data, with our findings demonstrating that MNV-1.CW1 I301 has increased cellular tropism in the spleen. Together, this work reveals the significance of the VP1 301 residue in MNV infectivity and pathogenesis.

Norovirus enters the gastrointestinal tract through transcystosis by M cells that are present at the epithelium of Peyer's patches and at the tips of intestinal villi (43), and once inside the gastrointestinal tract, viruses come into contact with immune cells, such as dendritic cells and macrophages. Our data suggests a mechanism whereby MNV-1.CW1 I301 has greater attachment and increased affinity to these cells, and thus a greater proportion of this virus disseminates throughout the host via immune cells to the spleen and other organs. MNV-1.CW1 T301, on the other hand, has lower binding affinity and infectivity to these cells, and thus more virus stays proximal to the gastrointestinal tract. It is also possible that similar amounts of MNV-1.CW1 I301 and MNV-1.CW1 T301 disseminates to the spleen, but then the MNV-1.CW1 I301 variant has increased replication once in splenic cells, due to the richness of immune cells present.

412 The binding of MNV to CD300lf is thought to be a low affinity, high avidity interaction
413 that requires a network of hydrophilic and hydrophobic interactions (25). Each virion
414 is thought to interact with multiple CD300lf receptors, forming clusters that increase
415 avidity (25, 44). Our results are consistent with this hypothesis and also suggest that
416 this high avidity interaction is dependent on membrane fluidity, with low temperature
417 and the depletion of cholesterol resulting in decreased virus binding. These results
418 build upon the established idea that cholesterol is required for MNV endocytosis and
419 further implicates the importance of lipid rafts (36, 45), which contain both cholesterol
420 and CD300lf, and are important in signal transduction (38, 46–48). Sphingolipid
421 biosynthesis is required to induce a conformational change in CD300lf to allow MNV
422 infection (48), and thus it can be postulated that sphingolipids may also be required
423 alongside cholesterol to regulate membrane fluidity required for lipid raft formation
424 (47, 48). As isoleucine at VP1 301 enhances binding to cells when in suspension,
425 one interpretation of our data is that increased hydrophobic interactions between the
426 VP1 I301 variant and CD300lf confers increased affinity with receptor clusters that
427 form at cholesterol-rich areas of the membrane. A similar interaction also occurs in
428 other viruses, such as influenza, with cholesterol inducing nano-clusters of the
429 glycosphingolipid receptor to increase virus infectivity (49). Furthermore, previous
430 work has shown that GCDCA and metal ions can induce MNV P domain
431 conformational changes that increase receptor affinity (6, 29). Future investigations
432 should therefore investigate whether these factors can have additive effects in MNV
433 attachment to suspension cells.
434 The results described in our study suggests that I301 plays a physiologically
435 important role. It must be noted, however, that a previous study suggested the T301I
436 substitution is a tissue culture adaptation, with MNV-3 collected from mice faeces 56

437 days post-infection reverting to T301 (15), which we did not observe in our
438 experiments. The difference in these findings may be explained by experimental
439 variations such as the location of infection, time post-infection, or both.
440 During infection of the host, viral quasi-species may provide the VP1 sequence
441 diversity to generate viral sub-populations that allow access to different host cell
442 types and widen dissemination. Furthermore, these sub-populations may change
443 over time, depending on host immune pressures. Indeed, the T301I substitution has
444 been previously identified as one of three mutations that occurred in an MNV escape
445 mutant, following the addition of a monoclonal antibody that targeted VP1 (50). Viral
446 quasi-species evolution is likely to be of relevance to HNV pathogenesis and chronic
447 infection. Chronic HNV infection can persist for years in immunocompromised
448 patients, leading to dehydration and nutrient deficiencies that can lead to mortality
449 (19, 20, 51). Evolutionary studies have shown that HNV amino acid mutations
450 accumulate throughout the chronic infection period (52, 53), with most being in the
451 VP1 P domain (53). These evolutionary changes have also been linked to immune
452 evasion, which leads to the changes in antigenic epitope of the virus (54). However,
453 data that utilises virus-like particles (VLPs) and bioinformatics are contradictory as to
454 whether this can change receptor-binding interactions (54, 55). Our study
455 demonstrates a mechanism by which virus capsid evolution can significantly affect
456 tissue tropism and susceptibility by enhancing interaction with the host cell. It can be
457 postulated that this mechanism may also be utilised by HNV to avoid immune
458 detection and influence chronic infection. This hypothesis should be investigated
459 further as current reverse genetics systems (56, 57) are improved to allow the study
460 of HNV infectivity.

Methods

Cells and mice

BHK-21 cells (obtained from ATCC) and RAW264.7 cells (gifted by Ian Clarke, University of Southampton) were maintained as previously described (6), with adherently grown BV-2 cells (gifted by Ian Goodfellow, University of Cambridge), maintained using the same method. Suspension grown BV-2 cells (referred to as BV-2S cells) were cultured in spinner flasks by maintaining a viable density of 0.5-1x10^6 cells/mL with media changes every 2 days. WEHI-231 cells (obtained from ATCC) were maintained as previously described (58). Cells were incubated at 37°C and 5% CO_2.

Balb/c mice were purchased from Jackson Laboratories (Bar Harbor, ME) and housed under specific-pathogen-free (SPF) and MNV-free conditions in accordance with federal and university guidelines. The protocol was approved by the University of Michigan Committee on Use and Care of Animals (UCUCA protocol number PRO00010484). Mice were allowed to acclimate in the facility for 6 days prior to infection. Mice were infected via oral gavage with 3x10^5 PFU of virus in 200 µL/mouse. Tissues were harvested at 12 hours post infection and processed for plaque assay as described (59).

Plasmid constructs

The plasmid, pT7-MNV*, containing the infectious clone sequence from MNV-1 strain CW1P3 (36) under control of T7 promoter was used for virus recovery. To exchange VP1 T301 standard two-step overlapping PCR mutagenesis was used with this plasmid as template (31). The pcDNA3.1(+)IRES GFP plasmid used for transfection experiments (kindly donated by Jamel Mankouri, University of Leeds)

has already been described (61). Sequences of plasmids and primers are available on request.

In vitro transcription and virus recovery

MNV plasmids were linearised with *Not*I and phenol/chloroform extracted before being used for *in vitro* transcription using the HiScribe™ T7 ARCA mRNA Kit (NEB), following the manufacturer's instructions. RNA was purified and concentrated using the RNA Clean and Concentrator Kit (Zymo). RNA/DNA transfection was carried out as previously described (62). GFP fluorescence at 24 and 48 hours post transfection was analysed via the Incucyte S3 machine (Sartorius).

$TCID_{50}$ assay

Viral infectivity was determined using a $TCID_{50}$ assay modified from Hwang et al (29), as per (6). For adherent $TCID_{50}$ assays, BV-2 cells were seeded into 96 well plates at $2x10^4$ cells/well and left overnight before infection. For suspension $TCID_{50}$ assays, viral dilutions were prepared and added to the plates first, prior to infection. $TCID_{50}$ values were calculated according to the Spearman and Kärber algorithm (30).

MTS assay

Cell viability in WEHI-231 cells was calculated 48 hours after MNV infection via the CellTiter 96® AQueous One Solution Cell Proliferation Assay kit, following manufacturer's instructions. Absorbance was read on the Infinite F50 (Tecan) machine. Cytopathic effect was assigned to wells with values under 1. The number of positive wells was then used to calculate $TCID_{50}$ values.

Plaque assay

The plaque assay was performed from virus isolated from mouse tissue as previously described (59, 63). Data were normalized to the tissue weight and expressed as PFU per gram of tissue.

MNV RNA extraction and sequencing

Viral RNA was extracted using the Direct-zol RNA miniprep kit (Zymo Research) according to the manufacturer's instructions. For VP1 sequencing, ORF2 was amplified by RT-PCR using Superscript IV (Invitrogen), followed by second strand synthesis using Phusion DNA Polymerase (NEB). The sequence of the amplicon was determined by Sanger sequencing (Azenta). Sequences of primers used are available on request.

One-step RT-qPCR

Virus sample was treated with 25 U/mL recombinant HS-Nuclease (MoBiTec) at 37□C for 30 minutes and viral RNA was extracted as previously described (62). RNA reverse transcription and cDNA amplification was then carried out by the GoTaq 1-Step RT-qPCR System (Promega), using established primers (31). CT values were converted to RNA copies/mL by analysing against a pT7-MNV* RNA standard curve of known values. The results were read using the Stratagene Mx3005P qPCR machine (Agilent Technologies).

Western blot

SDS-PAGE and western blot analysis was carried out as previously described (27). Primary antibodies used were anti-MNV VP1 monoclonal antibody (MABF2097, Sigma-Aldrich), anti-CD300lf monoclonal (MAB27881, R&D Systems), anti-GAPDH monocolonal (60004-1, ProteinTech) and anti-BSA monoclonal antibody (66201-1, ProteinTech). Polyclonal anti-mouse (PA1-84388, Invitrogen) and anti-rabbit (HAF008, R&D Systems) HRP conjugates were employed as a secondary antibody. Blots were analysed on the G:BOX Chemi XX6 machine (Syngene).

Flow cytometry

Detached adherent BV-2 cells or BV-2S cells ($2x10^6$/mL) were analysed for CD300lf expression using a flow cytometry protocol previously described (64), with anti-CD300lf primary antibody (MAB27881, R&D Systems) and Alexafluor647 goat Anti-mouse IgG (A-21235, Invitrogen). The samples were analysed on a Cytoflex S flow cytometer (Beckman Coulter).

Viral binding assay

Viral binding affinity to BV-S cells was determined using a binding assay modified from Berry and Tse (33). 10^5 BV-2S cells were pre-treated with 50 µM dynasore (Ds; Cambridge Bioscience), 2 mM MβCD (Sigma-Aldrich) or 40 mM Los (Sigma-Aldrich) for 30 minutes at 37□C. MNV was added to the cells at an MOI of 1 and incubated at either 0□C or 37□C for 2 hours, before completing the binding assay as described.

Statistics

Data were analysed and presented via GraphPad Prism v9.0 as mean ± SEM, N; biological repeat, with number of repeats stipulated in the figure legends. Statistical tests performed are also detailed within the figure legends with significant differences indicated by *p < 0.05; **p < 0.01; ***p < 0.001.

Author Contributions

Conceptualization: Jake T. Mills, Susanna C. Minogue, Joseph S. Snowden, David J. Rowlands, Nicola J. Stonehouse, Christiane E. Wobus and Morgan R. Herod.

Investigation: Jake T. Mills, Susanna C. Minogue, Joseph S. Snowden, Wynter K.C. Arden, and Morgan R. Herod.

Supervision: David J. Rowlands, Christiane E. Wobus and Morgan R. Herod

Writing – original draft: Jake T. Mills and Morgan R. Herod.

Writing – review & editing: Jake T. Mills, David J. Rowlands, Nicola J. Stonehouse, Christiane E. Wobus and Morgan R. Herod.

Acknowledgements

We thank Ian Goodfellow (University of Cambridge) and Ian Clarke (University of Southampton) for the murine cell lines.

Funding

This work was supported by funding to MRH from the MRC (MR/S007229/1). MRH, DJR and NJS were supported by the BBSRC (BB/T015748/1). JSS was funded by a Wellcome Trust studentship (102174/B/13/Z). Work in the laboratory of CEW was supported by NIH award R21AI154647. The funders had no role in study design, data collection and analysis, decision to publish, or preparation of the manuscript.

Conflicts of interest

The authors declare no conflicts of interest.

References

1. Patel MM, Widdowson M-A, Glass RI, Akazawa K, Vinjé J, Parashar UD. 2008. Systematic Literature Review of Role of Noroviruses in Sporadic Gastroenteritis. Emerg Infect Dis J 14:1224–1224.

2. Hardy ME. 2005. Norovirus protein structure and function. FEMS Microbiol Lett 253:1–8.

3. McFadden N, Bailey D, Carrara G, Benson A, Chaudhry Y, Shortland A, Heeney J, Yarovinsky F, Simmonds P, Macdonald A, Goodfellow I. 2011. Norovirus Regulation of the Innate Immune Response and Apoptosis Occurs via the Product of the Alternative Open Reading Frame 4. PLOS Pathog 7:e1002413.

4. Conley MJ, McElwee M, Azmi L, Gabrielsen M, Byron O, Goodfellow IG, Bhella D. 2019. Calicivirus VP2 forms a portal-like assembly following receptor engagement. Nature 565:377–381.

5. Turgay K, Anna K, S HG, K PJ. 2021. Structural Basis for Human Norovirus Capsid Binding to Bile Acids. J Virol 93:e01581-18.

6. Snowden JS, Hurdiss DL, Adeyemi OO, Ranson NA, Herod MR, Stonehouse NJ. 2020. Dynamics in the murine norovirus capsid revealed by high-resolution cryo-EM. PLOS Biol 18:e3000649.

7. Ettayebi K, Crawford SE, Murakami K, Broughman JR, Karandikar U, Tenge VR, Neill FH, Blutt SE, Zeng X-L, Qu L, Kou B, Opekun AR, Burrin D, Graham DY, Ramani S, Atmar RL, Estes MK. 2016. Replication of human noroviruses in stem cell-derived human enteroids. Science 353:1387–1393.

8. Mirabelli C, Jones MK, Young VL, Kolawole AO, Owusu I, Shan M, Abuaita B, Turula H, Trevino JG, Grigorova I, Lundy SK, Lyssiotis CA, Ward VK, Karst SM, Wobus CE. 2022. Human Norovirus Triggers Primary B Cell Immune Activation In Vitro. mBio 13:e0017522.

9. Ghosh S, Kumar M, Santiana M, Mishra A, Zhang M, Labayo H, Chibly AM, Nakamura H, Tanaka T, Henderson W, Lewis E, Voss O, Su Y, Belkaid Y, Chiorini JA, Hoffman MP, Altan-Bonnet N. 2022. Enteric viruses replicate in salivary glands and infect through saliva. Nature 607:345–350.

10. Green KY, Kaufman SS, Nagata BM, Chaimongkol N, Kim DY, Levenson EA, Tin CM, Yardley AB, Johnson JA, Barletta ABF, Khan KM, Yazigi NA, Subramanian S, Moturi SR, Fishbein TM, Moore IN, Sosnovtsev SV. 2020. Human norovirus targets enteroendocrine epithelial cells in the small intestine. Nat Commun 11:2759.

11. Hsu CC, Wobus CE, Steffen EK, Riley LK, Livingston RS. 2005. Development of a microsphere-based serologic multiplexed fluorescent immunoassay and a reverse transcriptase PCR assay to detect murine norovirus 1 infection in mice. Clin Diagn Lab Immunol 12:1145–1151.

12. Karst SM, Wobus CE, Lay M, Davidson J, Virgin HW. 2003. STAT1-Dependent Innate Immunity to a Norwalk-Like Virus. Science 299:1575–1575.

13. Wobus CE, Karst SM, Thackray LB, Chang K-O, Sosnovtsev SV, Belliot G, Krug A, Mackenzie JM, Green KY, Virgin HW. 2004. Replication of Norovirus in cell culture reveals a tropism for dendritic cells and macrophages. PLoS Biol, 2004/11/30 ed. 2:e432–e432.

14. Arias A, Bailey D, Chaudry Y, Goodfellow I. 2012. Development of a reverse-genetics system for murine norovirus 3: long-term persistence occurs in the caecum and colon. J Gen Virol 93:1432–1441.

15. Grau KR, Roth AN, Zhu S, Hernandez A, Colliou N, DiVita BB, Philip DT, Riffe C, Giasson B, Wallet SM, Mohamadzadeh M, Karst SM. 2017. The major targets of acute norovirus infection are immune cells in the gut-associated lymphoid tissue. Nat Microbiol 2:1586–1591.

16. Shortland A, Chettle J, Archer J, Wood K, Bailey D, Goodfellow I, Blacklaws BA, Heeney JL. 2014. Pathology caused by persistent murine norovirus infection. J Gen Virol 95:413–422.

17. Mumphrey SM, Changotra H, Moore TN, Heimann-Nichols ER, Wobus CE, Reilly MJ, Moghadamfalahi M, Shukla D, Karst SM. 2007. Murine norovirus 1 infection is associated with histopathological changes in immunocompetent hosts, but clinical disease is prevented by STAT1-dependent interferon responses. J Virol 81:3251–3263.

18. Van Winkle JA, Robinson BA, Peters AM, Li L, Nouboussi RV, Mack M, Nice TJ. 2018. Persistence of Systemic Murine Norovirus Is Maintained by Inflammatory Recruitment of Susceptible Myeloid Cells. Cell Host Microbe 24:665-676.e4.

19. Atmar RL, Opekun AR, Gilger MA, Estes MK, Crawford SE, Neill FH, Graham DY. 2008. Norwalk virus shedding after experimental human infection. Emerg Infect Dis 14:1553–1557.

638 20. Gallimore CI, Lewis D, Taylor C, Cant A, Gennery A, Gray JJ. 2004. Chronic
639 excretion of a norovirus in a child with cartilage hair hypoplasia (CHH). J Clin
640 Virol 30:196–204.

641 21. Wilen Craig B., Lee Sanghyun, Hsieh Leon L., Orchard Robert C., Desai
642 Chandni, Hykes Barry L., McAllaster Michael R., Balce Dale R., Feehley Taylor,
643 Brestoff Jonathan R., Hickey Christina A., Yokoyama Christine C., Wang Ya-
644 Ting, MacDuff Donna A., Kreamalmayer Darren, Howitt Michael R., Neil Jessica
645 A., Cadwell Ken, Allen Paul M., Handley Scott A., van Lookeren Campagne
646 Menno, Baldridge Megan T., Virgin Herbert W. 2018. Tropism for tuft cells
647 determines immune promotion of norovirus pathogenesis. Science 360:204–
648 208.

649 22. Strine MS, Alfajaro MM, Graziano VR, Song J, Hsieh LL, Hill R, Guo J,
650 VanDussen KL, Orchard RC, Baldridge MT, Lee S, Wilen CB. 2022. Tuft-cell-
651 intrinsic and -extrinsic mediators of norovirus tropism regulate viral immunity.
652 Cell Rep 41:111593.

653 23. Bailey D, Thackray LB, Goodfellow IG. 2008. A single amino acid substitution in
654 the murine norovirus capsid protein is sufficient for attenuation in vivo. J Virol,
655 2008/05/21 ed. 82:7725–7728.

656 24. Haga K, Fujimoto A, Takai-Todaka R, Miki M, Doan YH, Murakami K,
657 Yokoyama M, Murata K, Nakanishi A, Katayama K. 2016. Functional receptor
658 molecules CD300lf and CD300ld within the CD300 family enable murine
659 noroviruses to infect cells. Proc Natl Acad Sci 113:E6248.

660 25. Nelson CA, Wilen CB, Dai Y-N, Orchard RC, Kim AS, Stegeman RA, Hsieh LL,
661 Smith TJ, Virgin HW, Fremont DH. 2018. Structural basis for murine norovirus
662 engagement of bile acids and the CD300lf receptor. Proc Natl Acad Sci U S A,
663 2018/09/07 ed. 115:E9201–E9210.

664 26. Márquez JA, Galfré E, Dupeux F, Flot D, Moran O, Dimasi N. 2007. The crystal
665 structure of the extracellular domain of the inhibitor receptor expressed on
666 myeloid cells IREM-1. J Mol Biol 367:310–318.

667 27. Borrego F. 2013. The CD300 molecules: an emerging family of regulators of the
668 immune system. Blood 121:1951–1960.

669 28. Graziano VR, Walker FC, Kennedy EA, Wei J, Ettayebi K, Strine MS, Filler RB,
670 Hassan E, Hsieh LL, Kim AS, Kolawole AO, Wobus CE, Lindesmith LC, Baric
671 RS, Estes MK, Orchard RC, Baldridge MT, Wilen CB. 2020. CD300lf is the
672 primary physiologic receptor of murine norovirus but not human norovirus.
673 PLOS Pathog 16:e1008242.

674 29. B SM, N WA, Q SH, Christopher N, B WC, H FD, W VH, J ST, Susana L. 2021.
675 Bile Salts Alter the Mouse Norovirus Capsid Conformation: Possible
676 Implications for Cell Attachment and Immune Evasion. J Virol 93:e00970-19.

677 30. Sherman MB, Williams AN, Smith HQ, Pettitt BM, Wobus CE, Smith TJ. 2021.
678 Structural Studies on the Shapeshifting Murine Norovirus. Viruses 13:2162.

679 31. Helm EW, Peiper AM, Phillips M, Williams CG, Sherman MB, Kelley T, Smith
680 HQ, Jacobs SO, Shah D, Tatum SM, Iyer N, Grodzki M, Morales Aparicio JC,
681 Kennedy EA, Manzi MS, Baldridge MT, Smith TJ, Karst SM. 2022.

682 Environmentally-triggered contraction of the norovirus virion determines
683 diarrheagenic potential. Front Immunol 13:1043746.

684 32. Strong DW, Thackray LB, Smith TJ, Virgin HW. 2012. Protruding domain of
685 capsid protein is necessary and sufficient to determine murine norovirus
686 replication and pathogenesis in vivo. J Virol 86:2950–2958.

687 33. Zhu S, Watanabe M, Kirkpatrick E, Murray AB, Sok R, Karst SM. 2015.
688 Regulation of Norovirus Virulence by the VP1 Protruding Domain Correlates
689 with B Cell Infection Efficiency. J Virol 90:2858–2867.

690 34. Kilic T, Koromyslova A, Malak V, Hansman GS. 2018. Atomic Structure of the
691 Murine Norovirus Protruding Domain and Soluble CD300lf Receptor Complex. J
692 Virol 92:e00413-18.

693 35. Herod MR, Ward JC, Tuplin A, Harris M, Stonehouse NJ, McCormick CJ. 2022.
694 Positive strand RNA viruses differ in the constraints they place on the folding of
695 their negative strand. RNA N Y N 28:1359–1376.

696 36. Perry JW, Wobus CE. 2010. Endocytosis of murine norovirus 1 into murine
697 macrophages is dependent on dynamin II and cholesterol. J Virol, 2010/04/07
698 ed. 84:6163–6176.

699 37. Furlong K, Biering SB, Choi J, Wilen CB, Orchard RC, Wobus CE, Nelson CA,
700 Fremont DH, Baldridge MT, Randall G, Hwang S. 2020. CD300LF
701 Polymorphisms of Inbred Mouse Strains Confer Resistance to Murine Norovirus
702 Infection in a Cell Type-Dependent Manner. J Virol 94.

703 38. Lingemann M, Taube S. 2018. Open Sesame: New Keys to Unlocking the Gate
704 to Norovirus Infection. Cell Host Microbe 24:463–465.

705 39. Maloney JM, Lehnhardt E, Long AF, Vliet KJV. 2013. Mechanical Fluidity of
706 Fully Suspended Biological Cells. Biophys J 105:1767–1777.

707 40. Ben-Dov N, Korenstein R. 2013. Proton-induced endocytosis is dependent on
708 cell membrane fluidity, lipid-phase order and the membrane resting potential.
709 Biochim Biophys Acta BBA - Biomembr 1828:2672–2681.

710 41. Theodoropoulou E, Marsh D. 1999. Interactions of angiotensin II non-peptide
711 AT(1) antagonist losartan with phospholipid membranes studied by combined
712 use of differential scanning calorimetry and electron spin resonance
713 spectroscopy. Biochim Biophys Acta 1461:135–146.

714 42. Larbi A, Douziech N, Khalil A, Dupuis G, Gheraïri S, Guérard K-P, Fülöp TJ.
715 2004. Effects of methyl-beta-cyclodextrin on T lymphocytes lipid rafts with
716 aging. Exp Gerontol 39:551–558.

717 43. Gonzalez-Hernandez Mariam B., Liu Thomas, Blanco Luz P., Auble Heather,
718 Payne Hilary C., Wobus Christiane E. 2013. Murine Norovirus Transcytosis
719 across an In Vitro Polarized Murine Intestinal Epithelial Monolayer Is Mediated
720 by M-Like Cells. J Virol 87:12685–12693.

721 44. Koromyslova Anna D., Devant Jessica M., Kilic Turgay, Sabin Charles D.,
722 Malak Virginie, Hansman Grant S., Sandri-Goldin Rozanne M. Nanobody-
723 Mediated Neutralization Reveals an Achilles Heel for Norovirus. J Virol
724 94:e00660-20.

45. Gerondopoulos A, Jackson T, Monaghan P, Doyle N, Roberts LO. 2010. Murine norovirus-1 cell entry is mediated through a non-clathrin-, non-caveolae-, dynamin- and cholesterol-dependent pathway. J Gen Virol. Microbiology Society.

46. Pike LJ. 2003. Lipid rafts: bringing order to chaos. J Lipid Res 44:655–667.

47. García-Arribas AB, Alonso A, Goñi FM. 2016. Cholesterol interactions with ceramide and sphingomyelin. Prop Funct Cholest 199:26–34.

48. Orchard RC, Wilen CB, Virgin HW. 2018. Sphingolipid biosynthesis induces a conformational change in the murine norovirus receptor and facilitates viral infection. Nat Microbiol 3:1109–1114.

49. Goronzy IN, Rawle RJ, Boxer SG, Kasson PM. 2018. Cholesterol enhances influenza binding avidity by controlling nanoscale receptor clustering. Chem Sci 9:2340–2347.

50. Rotem A, Serohijos AWR, Chang CB, Wolfe JT, Fischer AE, Mehoke TS, Zhang H, Tao Y, Lloyd Ung W, Choi J-M, Rodrigues JV, Kolawole AO, Koehler SA, Wu S, Thielen PM, Cui N, Demirev PA, Giacobbi NS, Julian TR, Schwab K, Lin JS, Smith TJ, Pipas JM, Wobus CE, Feldman AB, Weitz DA, Shakhnovich EI. 2018. Evolution on the Biophysical Fitness Landscape of an RNA Virus. Mol Biol Evol 35:2390–2400.

51. Koo HL, DuPont HL. 2009. Noroviruses as a potential cause of protracted and lethal disease in immunocompromised patients. Clin Infect Dis Off Publ Infect Dis Soc Am 49:1069–1071.

747 52. Siebenga JJ, Beersma MFC, Vennema H, van Biezen P, Hartwig NJ,
748 Koopmans M. 2008. High prevalence of prolonged norovirus shedding and
749 illness among hospitalized patients: a model for in vivo molecular evolution. J
750 Infect Dis 198:994–1001.

751 53. Schorn R, Höhne M, Meerbach A, Bossart W, Wüthrich RP, Schreier E, Müller
752 NJ, Fehr T. 2010. Chronic norovirus infection after kidney transplantation:
753 molecular evidence for immune-driven viral evolution. Clin Infect Dis Off Publ
754 Infect Dis Soc Am 51:307–314.

755 54. Debbink K, Lindesmith LC, Ferris MT, Swanstrom J, Beltramello M, Corti D,
756 Lanzavecchia A, Baric RS. 2014. Within-host evolution results in antigenically
757 distinct GII.4 noroviruses. J Virol 88:7244–7255.

758 55. Doerflinger Sylvie Y., Weichert Stefan, Koromyslova Anna, Chan Martin,
759 Schwerk Christian, Adam Ruediger, Jennewein Stefan, Hansman Grant S.,
760 Schroten Horst. 2017. Human Norovirus Evolution in a Chronically Infected
761 Host. mSphere 2:e00352-16.

762 56. Oliveira LM, Blawid R, Orílio AF, Andrade BYG, Souza ACA, Nagata T. 2018.
763 Development of an infectious clone and replicon system of norovirus GII.4. J
764 Virol Methods 258:49–53.

765 57. Katayama K, Murakami K, Sharp TM, Guix S, Oka T, Takai-Todaka R,
766 Nakanishi A, Crawford SE, Atmar RL, Estes MK. 2014. Plasmid-based human
767 norovirus reverse genetics system produces reporter-tagged progeny virus
768 containing infectious genomic RNA. Proc Natl Acad Sci U S A 111:E4043-4052.

769 58. Hirai H, Adachi T, Tsubata T. 2004. Involvement of cell cycle progression in
770 survival signaling through CD40 in the B-lymphocyte line WEHI-231. Cell Death
771 Differ 11:261–269.

772 59. Turula H, Bragazzi Cunha J, Mainou BA, Ramakrishnan SK, Wilke CA,
773 Gonzalez-Hernandez MB, Pry A, Fava J, Bassis CM, Edelman J, Shah YM,
774 Corthesy B, Moore BB, Wobus CE. 2018. Natural Secretory Immunoglobulins
775 Promote Enteric Viral Infections. J Virol 92.

776 60. Ward VK, McCormick CJ, Clarke IN, Salim O, Wobus CE, Thackray LB, Virgin
777 HW, Lambden PR. 2007. Recovery of infectious murine norovirus using pol II-
778 driven expression of full-length cDNA. Proc Natl Acad Sci 104:11050.

779 61. Amako Y, Igloi Z, Mankouri J, Kazlauskas A, Saksela K, Dallas M, Peers C,
780 Harris M. 2013. Hepatitis C virus NS5A inhibits mixed lineage kinase 3 to block
781 apoptosis. J Biol Chem 288:24753–24763.

782 62. Herod MR, Gold S, Lasecka-Dykes L, Wright C, Ward JC, McLean TC, Forrest
783 S, Jackson T, Tuthill TJ, Rowlands DJ, Stonehouse NJ. 2017. Genetic economy
784 in picornaviruses: Foot-and-mouth disease virus replication exploits alternative
785 precursor cleavage pathways. PLoS Pathog 13:e1006666–e1006666.

786 63. 2012. Plaque assay for murine norovirus. United States.

787 64. Herod MR, Pineda RG, Mautner V, Onion D. 2015. Quantum Dot Labelling of
788 Adenovirus Allows Highly Sensitive Single Cell Flow and Imaging Cytometry.
789 Small 11:797–803.

790